

Organic thin-film solar cells with a Cu anode: Improvement of the photovoltaic properties on aging in air

Yuki Yoshida,¹ Senku Tanaka,¹ Yasuhisa Fujita,² and Ichiro Hiromitsu^{1,a)}

¹*Department of Material Science, Faculty of Science and Engineering, Shimane University, Matsue 690-8504, Japan*

²*Department of Electronic and Control Systems Engineering, Shimane University, Matsue 690-8504, Japan*

(Received 8 June 2009; accepted 20 August 2009; published online 24 September 2009)

The photovoltaic properties of a Ga-doped ZnO (GZO)/3,4,9,10-perylene-tetracarboxyl-bis-benzimidazole (PTCBI)/Zn-phthalocyanine (ZnPc)/Cu heterojunction cell (cell A) and a GZO/ZnPc/Cu Schottky-barrier cell (cell B) were investigated. The energy conversion efficiency η of cell A was only 0.02% immediately after the device preparation but improved to 0.46% after aging for 24 days in air. To elucidate the mechanism of this aging effect, photocurrent action and electro-absorption spectra were measured for cell B. The results reveal that a Schottky barrier exists at the ZnPc/Cu interface which blocks the transport of photogenerated holes to the Cu electrode, and the barrier height is reduced by a white-light illumination of the device after aging. The change in barrier height is attributed to the formation of electron traps at the surface of the ZnPc layer on aging that trap photogenerated electrons. © 2009 American Institute of Physics. [doi:10.1063/1.3226880]

I. INTRODUCTION

Organic thin-film solar cells are candidates for next-generation solar cells and have been extensively studied in recent years.^{1,2} The most widely studied organic thin-film solar cells are heterojunction³⁻⁶ and bulk-heterojunction cells⁷⁻¹⁰ made of two types of organic semiconductors, an electron donor and an acceptor. To improve the energy conversion efficiency of these cells, choice of the electrode materials and of the donor and acceptor is important. The Fermi level of the anode material should be close to the highest occupied molecular orbital (HOMO) level of the donor, and that of the cathode material should be close to the lowest unoccupied molecular orbital (LUMO) level of the acceptor.

We have recently reported on a heterojunction cell that uses a new type of transparent electrode Ga-doped ZnO(GZO).¹¹ The structure of the cell was GZO/3,4,9,10-perylene-tetracarboxyl-bis-benzimidazole (PTCBI)/Zn-phthalocyanine (ZnPc)/pentacene/Au, in which PTCBI is the acceptor, ZnPc is the donor, and pentacene is a buffer layer to prevent short circuit due to interpenetration of Au into the donor and acceptor layers. We showed that GZO is suitable for the cathode and indium tin oxide(ITO) is suitable for the anode. This difference between GZO and ITO is ascribed to the difference between their work functions, which are 4.4 eV (Ref. 11) and 4.7 eV (Ref. 12), respectively. GZO provides a new possibility for the design of organic thin-film solar cells.¹³ For example, the order of donor/acceptor stacking in the heterojunction cell can be inverted using GZO instead of ITO, which can change the amount of photon energy absorbed by the donor and acceptor layers. Another example is a Schottky-barrier cell made of a *p*-type organic semiconductor such as ZnPc. Using GZO, a Schottky barrier can be constructed at the transparent electrode/organic interface, thus increasing the amount of photon energy absorbed

at the depletion layer because it is located close to the transparent electrode. In our previous heterojunction device using Au as the top electrode, however, a pentacene buffer layer of ~100 nm in thickness was necessary to prevent short circuit. Such a thick buffer layer increases the series resistance of the device, resulting in a decrease in the short-circuit current and the fill factor. Thus, an anode material other than Au that can be used without any buffer layer is required to improve the energy conversion efficiency of GZO-based solar cells.

Here we report on the photovoltaic properties of organic cells using a Cu film as the anode. The Cu anode can be used without any buffer layer and a GZO/PTCBI/ZnPc/Cu heterojunction cell exhibited higher energy conversion efficiency than the previously reported GZO/PTCBI/ZnPc/pentacene/Au cell. Furthermore, the present GZO/PTCBI/ZnPc/Cu cell showed a drastic improvement in photovoltaic properties after aging in open air. We reported a similar aging effect for the GZO/PTCBI/ZnPc/pentacene/Au cell, but the effect is much more significant for the present device. Detailed results are presented for a simpler GZO/ZnPc/Cu Schottky-junction cell that indicate the mechanism of this aging effect.

II. EXPERIMENTAL

A. Sample preparation

ZnPc was purchased from Kanto Chem. Co. and PTCBI was synthesized using a literature procedure.¹⁴ These chemicals were sublimed under vacuum three times before use. The GZO film was deposited on a quartz substrate ($9 \times 24 \times 1$ mm³) by rf magnetron sputtering from a GZO ceramic target with a Ga content of 3.3 at. % (AGC Ceramics). The substrate temperature during deposition was 300 °C. The film thickness of the GZO film was estimated to be ~200 nm from interference peaks in the optical absorption

^{a)}Electronic mail: hiromitu@riko.shimane-u.ac.jp.

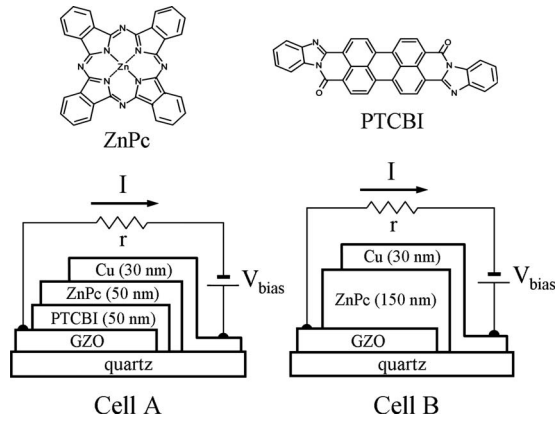


FIG. 1. Molecular structures of PTCBI and ZnPc, and schemes for cell A (GZO/PTCBI/ZnPc/Au) and cell B (GZO/ZnPc/Au). The electrical circuits for current-voltage measurement are also shown. The positive directions of the current I and the bias voltage V_{bias} are defined.

spectrum. The sheet resistance of the GZO film was $35 \text{ } \Omega/\text{sq}$, and the transmissivity for visible light was greater than $\sim 90\%$.

Two types of organic thin-film solar cells, a GZO/PTCBI(50 nm)/ZnPc(50 nm)/Cu(30 nm) heterojunction cell (cell A) and a GZO/ZnPc(150 nm)/Cu(30 nm) Schottky-junction cell (cell B), were prepared. Figure 1 shows diagrams of the cells and the molecular structures of ZnPc and PTCBI. All films except GZO were prepared by vacuum evaporation under a pressure of 1×10^{-4} Pa. The evaporation speed were 0.1 nm/s for PTCBI and ZnPc and 0.01 nm/s for Cu, as monitored by a quartz oscillator (ULVAC CRTM-5000 or CRTM-6000). The active area of the device was 0.3 cm^2 .

B. Dark current and photocurrent measurements

The electrical circuit for current-voltage measurement is shown in Fig. 1. The positive directions of the current I and the applied bias voltage V_{bias} as defined in Fig. 1 correspond to the directions of the forward current and the forward bias voltage. The current was measured from the voltage drop across a small resistance r . Photocurrent-voltage measurements were carried out under illumination of $100 \text{ mW}/\text{cm}^2$ with a spectrum of AM 1.5, which was obtained using a 300 W Xe lamp and home-made optical filters with an appropriate absorption spectrum. Photocurrent action (PA) spectra were measured using a 50 W halogen lamp as light source followed by a monochromator. The intensity of the monochromatic light obtained was of the order of $1 \text{ } \mu\text{W}$. Light was chopped with a frequency of 12 Hz, and the synchronous change in the photocurrent was detected using a lock-in amplifier. All measurements were carried out under vacuum at room temperature.

C. Electroabsorption measurement

The internal electric field of cell B was investigated using an electroabsorption (EA) technique.^{15,16} Electric-field modulation was applied to the device and the synchronous change in optical absorption coefficient was detected. Electric-field modulation of 1 Hz was applied to the device

using a function generator with an output signal of $V_m \sin \omega_m t$ with $V_m = 1$ or 2 V. The probe light for EA measurements was entered normally to the active area of the device from the Cu side. The light source was the same as for the PA spectra, but with no light chopper. The transmitted light intensity T was detected using a photomultiplier tube. The amplitude of the change in transmitted light intensity, ΔT , with frequency ω_m was detected using a lock-in amplifier. Then $-\Delta T/T$ is proportional to the change in optical absorption coefficient according to^{15,16}

$$-\frac{\Delta T}{T} \propto E_0 \times E_m \text{Im } \chi^{(3)}, \quad (1)$$

where E_0 , E_m , and $\text{Im } \chi^{(3)}$ are the static internal electric field, the amplitude of the modulation electric field, and the imaginary part of the third-order electric susceptibility, respectively, for the organic layer. Measurements were carried out under vacuum at room temperature.

III. RESULTS

A. Cell A: GZO/PTCBI/ZnPc/Cu

Using Cu as the top electrode, the device was free from short circuit, even without any buffer layer between the electrode and the ZnPc layer. This is in contrast to Au as top electrode, for which a buffer layer of ~ 100 nm in thickness was necessary to prevent short circuit.¹¹ The difference between Cu and Au electrodes can be explained by the following simplified model. During vacuum deposition, a metal atom of mass m impinges normally into an organic layer with an initial velocity of v_0 . In the organic layer, a resistive force $-bv$ is applied to the metal atom, where v is the velocity of the metal atom and b is a constant. By solving the equation of motion for the metal atom, the penetration depth can be calculated as mv_0/b . Thus, the penetration depth is determined by the momentum mv_0 of the metal atom as well as the constant b . Following the Maxwell-Boltzmann distribution, the momentum $\langle mv_0 \rangle$ becomes $(8mk_B T/\pi)^{1/2}$, where T is the deposition temperature and k_B is Boltzmann's constant. The atomic weights of Cu and Au are 64 and 197, respectively, and the deposition temperatures for Cu and Au are nearly the same, so the Cu atom has a substantially smaller momentum $\langle mv_0 \rangle$ compared to the Au atom. This explains the smaller penetration depth for Cu. Furthermore, the value of b might be greater for Cu than for Au if ZnPc molecules interact more strongly with Cu than with Au atoms.

Figure 2(a) shows the photocurrent density (J_{photo}) of cell A as a function of the bias voltage V_{bias} . Immediately after preparation, the cell showed poor photovoltaic properties: short-circuit current density $J_{\text{sc}} = 0.37 \text{ mA}/\text{cm}^2$, open circuit voltage $V_{\text{oc}} = 0.31 \text{ V}$, fill factor $\text{FF} = 0.17$, and energy conversion efficiency $\eta = 0.02\%$. After aging the device for 2 days in open air, however, the photovoltaic properties significantly improved. After aging for 24 days, a further improvement was observed ($J_{\text{sc}} = 2.7 \text{ mA}/\text{cm}^2$, $V_{\text{oc}} = 0.43 \text{ V}$, $\text{FF} = 0.40$, and $\eta = 0.46\%$). A similar aging effect was observed for GZO/PTCBI/ZnPc/pentacene/Au, with η increased by a factor of 1.9 after aging for 2 months in open air.¹¹ However,

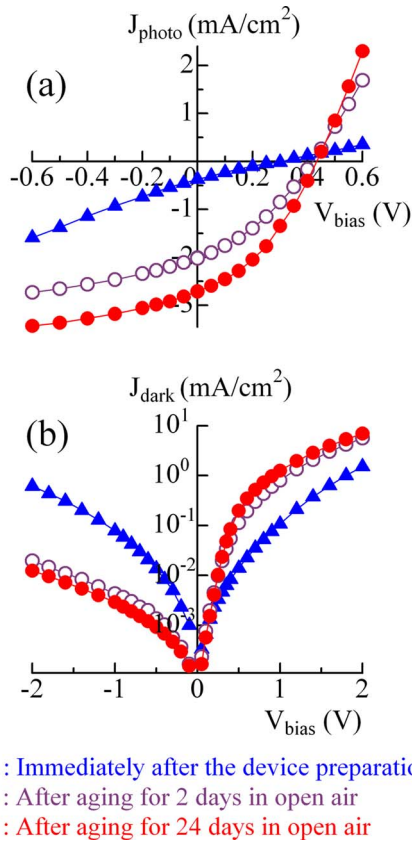


FIG. 2. (Color online) Bias voltage dependence of the current density of cell A (a) under white-light illumination from the GZO side using a light source of AM 1.5 and 100 mW/cm² and (b) in the dark immediately after the measurement for (a).

the aging effect is much greater for the present device, with η increased by a factor of 23 after aging for 24 days. The final efficiency of $\eta=0.46\%$ for cell A is much greater than $\eta=0.19\%$ for the previous GZO/PTCBI/ZnPc/pentacene/Au system. The higher efficiency of the present system can be attributed to the absence of a pentacene buffer layer.

Figure 2(b) shows the bias dependence of the dark current density for cell A. Immediately after the device preparation, J_{dark} at $V_{\text{bias}}=+2$ V was 1.5 mA/cm² and the rectification ratio at V_{bias} of ± 2 V was 2.5. After aging for 24 days, these values increased to 7.0 mA/cm² and 580, respectively. By contrast, the reverse J_{dark} decreased after aging.

A similar experiment was performed for a heterojunction device using Ni or Fe for the top electrode instead of Cu. The efficiency immediately after device preparation was 0.02% for both the Ni and Fe anodes and increased to 0.10% for Ni and 0.09% for Fe after aging for 10 days in air. Thus, the aging effect was greatest when the top electrode was Cu. This suggests that the ZnPc/Cu interface plays an important role in the aging effect for cell A. Hence, a detailed study was performed for a simpler system, cell B, to elucidate the mechanism of the aging effect.

B. Cell B: GZO/ZnPc/Cu

Figure 3 shows the current-voltage characteristics of cell B under white-light illumination and in the dark. An aging effect similar to that for cell A is observed. After aging for 3

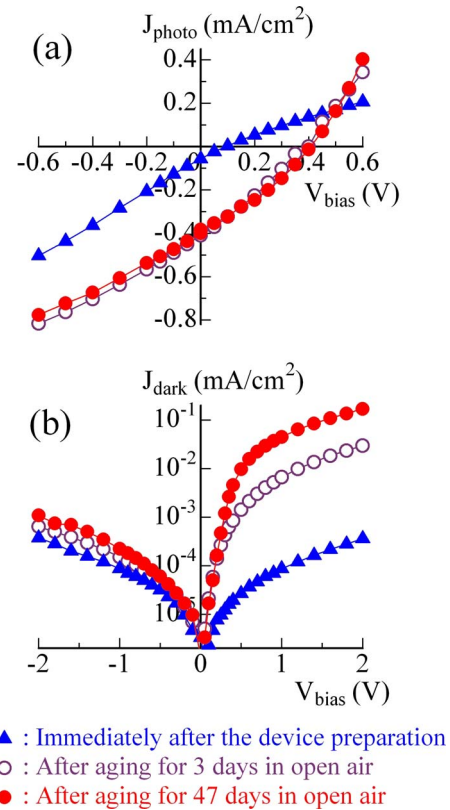


FIG. 3. (Color online) Bias voltage dependence of the current density of cell B (a) under white-light illumination from the GZO side using a light source of AM 1.5 and 100 mW/cm² and (b) in the dark immediately after the measurement for (a).

days in open air, the efficiency of cell B increased to 0.045% from an initial value of 0.001% for the as-prepared device, and the rectification ratio at V_{bias} of ± 2 V increased to 46 from an initial value of 0.96. After aging for 47 days, η and the rectification ratio further increased to 0.050% and 155, respectively. When the device was aged for 4 days in vacuum instead of air, no substantial increases in η and the rectification ratio were observed.

Next, PA spectra for cell B are presented for the following four cases.

Case 1: Immediately after device preparation.

Case 2: After illumination of a white light of 100 mW/cm² on the as-prepared device.

Case 3: After aging the device in air.

Case 4: After illumination of a white light of 100 mW/cm² on the aged device.

Figure 4(a) shows the PA spectra for cell B immediately after preparation (case 1). When the device was illuminated from the GZO side, the sign of the photocurrent depended on the wavelength, i.e., $\text{IPCE} < 0$ for $570 \text{ nm} < \lambda < 720 \text{ nm}$, and $\text{IPCE} > 0$ for $\lambda < 570 \text{ nm}$ or $\lambda > 720 \text{ nm}$, where IPCE is the incident photon-to-current conversion efficiency. When illuminated from the Cu side, positive IPCE values were observed for the whole wavelength region measured.

These results are explained by the coexistence of two Schottky barriers at the GZO/ZnPc and ZnPc/Cu interfaces.

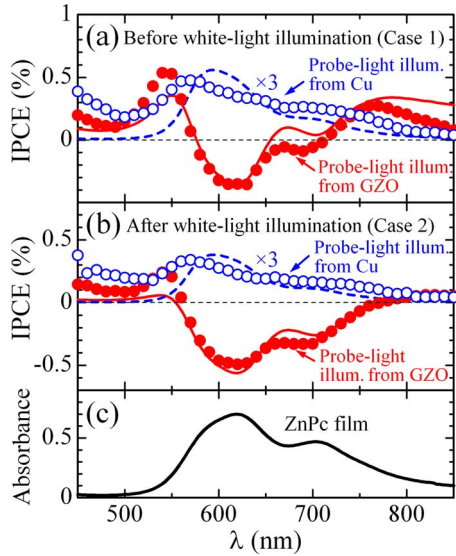


FIG. 4. (Color online) [(a) and (b)] PA spectra of cell B immediately after device preparation (a) before and (b) after illumination by white light of 100 mW/cm^2 for 20 min in vacuum from the GZO side of the as-prepared device ($V_{\text{bias}} = 0 \text{ V}$). The monochromatic probe light for PA measurement was illuminated either from the GZO or Cu sides. The IPCE values for illumination from the Cu side were enlarged by a factor of 3. The solid and broken lines in (a) and (b) are the theoretical ones with the values of parameters listed in Table I. (c) Optical absorption spectrum of a ZnPc film of 100 nm in thickness.

The two Schottky barriers correspond to two regions with photocurrent activity, as shown in Fig. 5. Photocurrent is generated by optical excitation of ZnPc in these regions, but the sign of the photocurrents generated in these two regions is opposite, i.e., negative for region I located near the GZO/ZnPc interface and positive for region II near the ZnPc/Cu interface, because the internal electric fields in these two regions are opposite in direction to each other.

Using the model shown in Fig. 5, the theoretical PA spectrum can be calculated in the following manner. When the device is illuminated from the GZO side, the proportion of incident photons absorbed by region I is

$$P_I = T_{\text{GZO}} [1 - \exp(-\alpha \times d_I)], \quad (2)$$

where T_{GZO} is the transmissivity of the GZO film, α is the optical absorption coefficient of the ZnPc layer, which can be calculated from the optical absorption spectrum in Fig. 4(c), and d_I is the thickness of region I. Similarly, the proportion

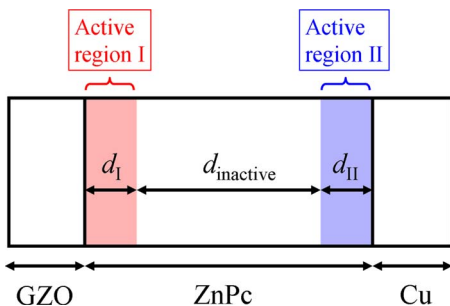


FIG. 5. (Color online) Model for the simulation of PA spectra for cell B. Two photocurrent-active regions I and II coexist in the ZnPc layer. The signs of the photocurrents generated in regions I and II are negative and positive, respectively.

TABLE I. Quantum efficiencies Φ_I and Φ_{II} for active regions I and II of the GZO/ZnPc/Cu cell (cell B) obtained by simulation of the IPCE spectra shown in Figs. 4 and 6. The width of the active regions I and II was fixed to 20 nm in the simulation, so that the estimated values of Φ_I and Φ_{II} are interpreted as the carrier-generation activities of the corresponding regions.

	Φ_I	Φ_{II}	IPCE spectrum
Immediately after device preparation			
Before white-light illumination (case 1)	0.032	0.14	Figure 4(a)
After white-light illumination for 20 min (case 2)	0.030	0.060	Figure 4(b)
After aging for 3 months in air			
Before white-light illumination (case 3)	0.016	0.12	Figure 6(a)
After white-light illumination for 20 min (case 4)	0.18	0.020	Figure 6(b)

of the incident photons absorbed by the active region II is

$$P_{II} = T_{\text{GZO}} \exp[-\alpha(d_I + d_{\text{inactive}})] \times [1 - \exp(-\alpha d_{II})], \quad (3)$$

where d_{II} and d_{inactive} are the thicknesses of region II and the inactive region in the ZnPc layer, respectively, as defined in Fig. 5. The IPCE is calculated as

$$\text{IPCE} = -\Phi_I \times P_I + \Phi_{II} \times P_{II}, \quad (4)$$

where Φ_I and Φ_{II} are the quantum efficiencies for photocurrent generation in regions I and II, respectively. Generally, Φ_I and Φ_{II} differ because the strength of the electric field in the two active regions is different and because the carrier-transport efficiency at the GZO/ZnPc and ZnPc/Cu interfaces differs. In the present calculation, it was assumed that Φ_I and Φ_{II} are independent of the excitation wavelength.

When illuminated from the Cu side, P_I and P_{II} are as follows:

$$P_I = T_{\text{Cu}} \exp[-\alpha(d_{II} + d_{\text{inactive}})] \times [1 - \exp(-\alpha \times d_I)], \quad (5)$$

$$P_{II} = T_{\text{Cu}} [1 - \exp(-\alpha \times d_{II})], \quad (6)$$

where T_{Cu} is the transmissivity of the Cu film.

The calculated PA spectra are shown in Fig. 4(a). In calculations, it was found that the spectral line shape was insensitive to the values of d_I and d_{II} , so that these values were fixed to 20 nm. The agreement between experimental and calculated values is satisfactory, as observed in Fig. 4(a). The estimated values of the quantum efficiencies Φ_I and Φ_{II} are 0.032 and 0.14, respectively (Table I). Since the values of d_I and d_{II} were fixed in the present simulation, the estimated values of Φ_I and Φ_{II} virtually include information on d_I and d_{II} and can be interpreted as the carrier-generation activity of regions I and II, respectively. Thus, the relation $\Phi_I < \Phi_{II}$ indicates that region II is more active than region I in the as-prepared device.

Figure 4(b) shows the PA spectra after an illumination of a white light of 100 mW/cm^2 for 20 min in vacuum (case 2). The spectral line shape resembles that before illumination [Fig. 4(a)], except that the wavelength region for negative IPCE for the probe-light illumination from the GZO side

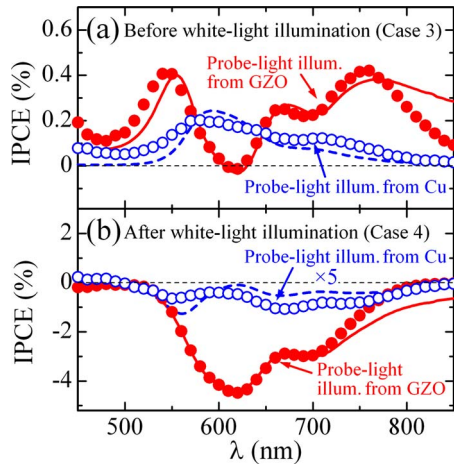


FIG. 6. (Color online) PA spectra for cell B after aging for 3 months in open air (a) before and (b) after illumination by white light of 100 mW/cm^2 for 20 min in vacuum from the GZO side of the aged device ($V_{\text{bias}}=0 \text{ V}$). The monochromatic probe light for the PA measurement was illuminated either from the GZO or Cu side. The IPCE value for the probe-light illumination from the Cu side in (b) was enlarged by a factor of 5. The solid and broken lines are the theoretical ones with the values of parameters listed in Table I.

extends to 800 nm. Estimated values of Φ_{I} and Φ_{II} are 0.030 and 0.060, respectively. In comparison to the values for case 1, Φ_{II} is smaller indicating that the carrier-generation activity of region II decreased on illumination.

Figure 6(a) shows the PA spectra of cell B after aging for 3 months in air (case 3). The IPCE sign is positive for probe-light illumination from both the GZO and Cu sides. This indicates that carrier generation mainly occurs in region II. The estimated values of Φ_{I} and Φ_{II} are 0.016 and 0.12, respectively.

After white-light illumination of the aged cell (case 4), PA spectra showed a surprising change [Fig. 6(b)]. The IPCE sign changed to negative after illumination for both directions of probe illumination. This indicates that carrier generation in case 4 mainly occurs in region I. The estimated values of Φ_{I} and Φ_{II} are 0.18 and 0.020, respectively. A decrease in Φ_{II} on illumination was also observed for case 2, but the effect was much more drastic for case 4. The IPCE sign recovered to positive when the aged device was kept in the dark, with a time constant of $\sim 1 \text{ h}$ in air and $\sim 10 \text{ h}$ in vacuum. Thus, the state of the aged device generating a negative photocurrent in case 4 is not stable in the dark.

In the next step, EA measurement was carried out for cell B to elucidate the features of the internal electric field in the ZnPc layer. The EA signal intensity is given by Eq. (1). Since $\text{Im} \chi^{(3)}$ is an extensive quantity, $-\Delta T/T$ satisfies the following relationship:

$$-\frac{\Delta T}{T} \propto (-E_{\text{I}} \times W_{\text{I}} + E_{\text{II}} \times W_{\text{II}}) \times E_m \\ = (-V_{\text{I}} + V_{\text{II}}) \times E_m, \quad (7)$$

where $E_{\text{I(II)}}$, $W_{\text{I(II)}}$, and $V_{\text{I(II)}}$ are the internal electric field, width, and diffusion potential, respectively, of depletion layer I (or II). Equation (7) takes into account the fact that the electric fields in depletion layers I and II are opposite in direction. It is assumed in Eq. (7) that the modulation

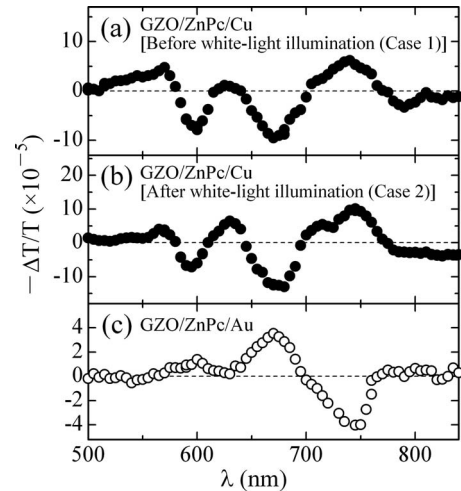


FIG. 7. [(a) and (b)] EA spectra for cell B immediately after device preparation (a) before and (b) after illumination by white light of 100 mW/cm^2 for 20 min in vacuum from the GZO side of the as-prepared device. (c) EA spectrum of a GZO/ZnPc(140 nm)/Au(15 nm) cell. $V_{\text{bias}}=0 \text{ V}$ for all spectra.

electric fields applied to depletion layers I and II have the same amplitude E_m . This assumption should be satisfied if the two depletion layers have the same dielectric constant and the same resistivity.

Figure 7(a) shows the EA spectrum of cell B immediately after device preparation (case 1). The line shape of the EA spectrum is close to the second derivative of the optical absorption spectrum of ZnPc, indicating that excitons generated in the ZnPc layer are weakly bound charge-transfer excitons.¹⁷ Figure 7(c) shows an EA spectrum of a GZO/ZnPc/Au cell. Comparison of Figs. 7(a) and 7(c) reveals that the sign of the EA signal is different between the two cases. According to Eq. (7), this indicates that the sign of $V_{\text{II}}-V_{\text{I}}$ for cell B is opposite to that for GZO/ZnPc/Au. In the latter case, the ZnPc/Au junction is nearly Ohmic,¹⁸⁻²⁰ whereas a Schottky barrier is formed at the GZO/ZnPc junction.¹¹ Hence, $V_{\text{II}} \approx 0$ and $V_{\text{I}} > 0$, so that $V_{\text{II}}-V_{\text{I}} < 0$ for GZO/ZnPc/Au. By contrast, $V_{\text{II}}-V_{\text{I}} > 0$ for cell B. This is consistent with the results of PA simulation in Table I; i.e., region II is more active than region I for case 1.

Figure 7(b) shows the EA spectrum of cell B after illumination of a white light of 100 mW/cm^2 for 20 min in vacuum (case 2). The sign and line shape of this spectrum are the same as for case 1 [Fig. 7(a)]. This indicates that $V_{\text{II}}-V_{\text{I}} > 0$ is satisfied even in case 2, in agreement with the result in Table I.

Figure 8(a) shows the EA spectrum for cell B after aging for 3 months in open air (case 3). The sign and line shape of the spectrum are the same as for case 1, indicating that $V_{\text{II}}-V_{\text{I}} > 0$ is still satisfied. Again, this is consistent with the result in Table I. However, after illumination of a white light of 100 mW/cm^2 for 20 min in vacuum (case 4), the line shape of the EA spectrum changed significantly [Fig. 8(b)]. The EA spectra in cases 1-3 [Figs. 7(a), 7(b), and 8(a)] are assigned to the bulk of the ZnPc layer.^{18,21,22} The EA spectrum in Fig. 8(b), on the other hand, differs in shape from the bulk spectrum, indicating that it contains a major contribu-

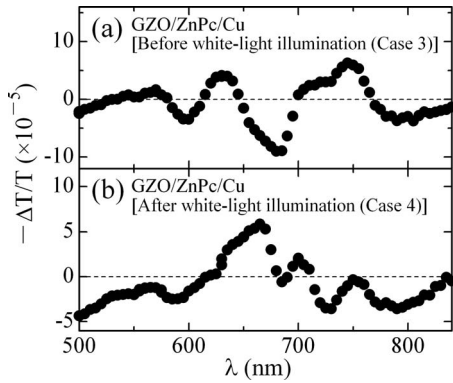


FIG. 8. EA spectra for cell B after aging for 3 months in open air (a) before and (b) after illumination by white light of 100 mW/cm^2 for 20 min in vacuum from the GZO side of the aged device ($V_{\text{bias}}=0 \text{ V}$).

tion from the surface of the ZnPc layer because the EA spectrum for the surface of an organic layer usually has a different line shape than that for the bulk.^{16,21,23}

IV. DISCUSSION

A. Mechanism of the aging effect for cell B

The results for cell B presented in Sec. III are summarized as follows.

- (1) The energy conversion efficiency under illumination of a white light of 100 mW/cm^2 was significantly improved by aging of the device in open air. The short-circuit current was always negative under the white-light illumination from the GZO side.
- (2) The forward dark current significantly increased after aging in air, whereas the reverse current showed a much smaller increase on aging.
- (3) The PA spectra indicated a coexistence of two photocurrent-active regions I and II located near the GZO/ZnPc and ZnPc/Cu interfaces. The photocurrents generated in the two regions have opposite directions to each other.
- (4) In case 1, the carrier-generation activity of region II was greater than that of region I. In case 2, the activity of region II was lower than that in case 1 but was still greater than the activity of region I.
- (5) In case 3, the activity of region I was negligible and nearly all the photocurrent was generated in region II. In case 4, however, the situation drastically changed: the activity of region I increased and that of region II was negligible.
- (6) The sign of the EA signal indicates that in cases 1–3 the diffusion potential of depletion layer II near the ZnPc/Cu interface was greater than that of depletion layer I near the GZO/ZnPc interface.
- (7) In case 4, the line shape of the EA spectrum was significantly different from that in the other cases, which is attributed to an increase in the EA signal from the surface of the ZnPc layer.

These results are explained based on the band diagrams shown in Fig. 9, in which two Schottky barriers exist at both

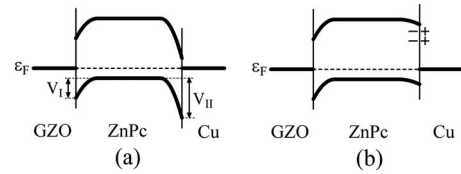


FIG. 9. Proposed energy band diagrams for cell B for $V_{\text{bias}}=0 \text{ V}$. V_I and V_{II} are the diffusion potentials of the two depletion layers near the GZO/ZnPc and ZnPc/Cu interfaces, respectively. (a) Cases 1–3 ($V_I < V_{II}$) although the values of V_I and V_{II} might be different among the three cases. (b) Case 4 ($V_I > V_{II}$).

sides of the ZnPc layer. Each Schottky barrier has an associated band bending region, i.e., a depletion layer near the surface, which corresponds to region I or II with photocurrent activity. Since the slopes of the bands for depletion layers I and II have opposite signs to each other, the directions of the electric fields in these two regions, as well as the directions of the photocurrents generated, are opposite to each other.

In case 1, the Schottky-barrier height at the ZnPc/Cu interface is higher than that at the GZO/ZnPc interface [Fig. 9(a)] and thus V_{II} is greater than V_I . This explains the higher carrier-generation activity of region II in case 1. The situation is similar in cases 2 and 3. The higher Schottky-barrier height at the ZnPc/Cu interface compared to that at the GZO/ZnPc interface is not explained by the reported work functions of GZO and Cu, which are 4.4 (Ref. 11) and 4.65 (Ref. 24), respectively. Thus, some type of vacuum-level shift is likely in cases 1–3 at the ZnPc/Cu and/or GZO/ZnPc interfaces, although a detailed mechanism for this shift is not yet known.

In case 4, the Schottky-barrier height at the ZnPc/Cu interface and the diffusion potential V_{II} significantly decreased, as shown in Fig. 9(b). As a result, the activity of region II is significantly lower. By contrast, the activity of region I increased because hole transport from region I to the Cu electrode is easier due to the decrease in blocking electric field in region II. It might be expected that the electric field in region I should be detected by EA in this case because V_{II} is small. This does not happen, however, because the EA signal from the surface of the ZnPc layer masks the EA signal from the bulk in case 4. The increase in surface EA signal is attributed to generation of an electric dipole layer at the ZnPc/Cu interface, as discussed in Sec. IV B.

As shown in Table I, the activity of region II is less for case 2 than for case 1, and the activity of region I is less for case 3 than for case 1. These differences are probably caused by a change in V_{II} or V_I . However, such changes cannot be detected by EA for the following reasons. In a previous study of Au/ZnPc/Al Schottky-barrier cell,¹⁸ we showed that (1) the standard depletion capacitance theory²⁵ applies to the ZnPc film and (2) the modulation voltage $V_m \sin \omega_m t$ applied during EA measurement is supplied only to the depletion layers if the modulation frequency is as low as 1 Hz. As shown in Eq. (7), the sensitivity of the EA measurement is determined by the amplitude of the modulation electric field E_m in the depletion layers. Because of the result (2) mentioned above, E_m for cell B is $V_m/(W_I + W_{II})$, where W_I and

W_{II} are the widths of the depletion layers I and II, respectively. From the depletion capacitance theory,²⁵ $W_{\text{I(or II)}}$ is proportional to $[V_{\text{I(or II)}}/N_{\text{I(or II)}}]^{1/2}$, where $N_{\text{I(or II)}}$ is the density of the localized negative charges in depletion layer I (or II). Thus, E_m can be expressed as

$$E_m \propto \frac{V_m}{\sqrt{V_{\text{I}}/N_{\text{I}}} + \sqrt{V_{\text{II}}/N_{\text{II}}}}. \quad (8)$$

E_m , or the sensitivity of EA measurement, changes if V_{I} , V_{II} , N_{I} , and N_{II} change. For example, if V_{I} is smaller for case 3 than for case 1, the sensitivity for V_{I} detection is expected to be greater for case 3. However, N_{I} might be changed by device aging. Because we do not know the value of N_{I} , the difference in sensitivity for the two cases is not known. Furthermore, if the GZO/ZnPc or ZnPc/Cu interface has large resistance, some of the modulation voltage is fed to the interface and the situation becomes more complicated. Thus, it is not possible to obtain reliable information about the difference in diffusion potential for different cases from EA measurements.

The band diagrams in Fig. 9 can explain the improvements in η and rectification ratio on aging, observed in Fig. 3. The photocurrent-voltage characteristics in Fig. 3(a) were measured under illumination of a white light of 100 mW/cm² from the GZO side, so that the band diagrams for cases 2 and 4 should apply in interpreting the experimental results in Fig. 3(a) for the as-prepared and aged devices, respectively. For the as-prepared device, a negative short-circuit current was observed under the white-light illumination from the GZO side although the conversion efficiency was very poor. In this case, the band diagram for case 2 [Fig. 9(a)] applies. Since the experimental conditions correspond to those for the PA spectrum with the probe-light illumination from the GZO side shown in Fig. 4(b), a negative short-circuit current is generated. However, because of the electric field in depletion layer II near the ZnPc/Cu interface, the negative photocurrent generated in region I is largely blocked and a positive photocurrent is generated in region II that cancels the negative photocurrent generated in region I. As a result, the conversion efficiency is poor. By contrast, after aging, the band diagram for case 4 [Fig. 9(b)] applies. In this case, the electric field near the ZnPc/Cu interface is significantly reduced, resulting in an increase in the negative photocurrent generated in region I and a decrease in the positive photocurrent generated in region II. Thus, the conversion efficiency is improved. Next, current-voltage measurements in the dark [Fig. 3(b)] are considered. Measurement was carried out immediately after white-light illumination, so that the device was in a state corresponding to case 2 or case 4. For the as-prepared device, the band diagram for case 2 [Fig. 9(a)] applies. In this case, hole injection from the Cu electrode under the forward bias is blocked by the tall Schottky barrier at the ZnPc/Cu interface, resulting in a small forward current. After aging, the band diagram for case 4 [Fig. 9(b)] applies. In this case, hole injection from the Cu electrode is enhanced because the Schottky-barrier height at the ZnPc/Cu interface is lower. As a result, the forward dark current is enhanced. Under reverse bias, the dark current is determined

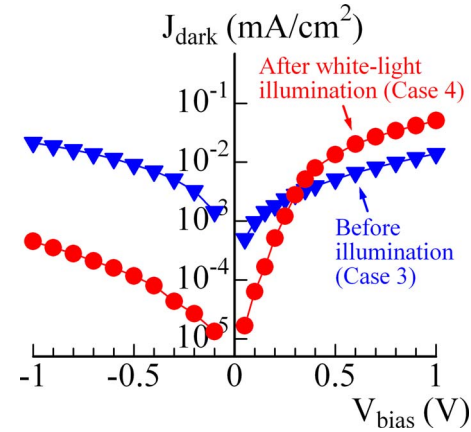


FIG. 10. (Color online) Dark current density vs applied bias voltage for cell B after aging for 4 months in air.

mainly by hole injection from GZO. Because the reverse dark current in Fig. 3(b) is not significantly affected by aging, the Schottky-barrier height at the GZO/ZnPc interface should be nearly the same for cases 4 and 2.

Case 3 is expressed by the band diagram in Fig. 9(a) and the rectification ratio is expected to be poor because the Schottky-barrier height at the ZnPc/Cu interface is greater than that at the GZO/ZnPc interface. This was actually observed, as shown in Fig. 10, and the forward current density for $V_{\text{bias}} > 0.4$ V in case 3 was less than that in case 4. This can be explained by the tall Schottky barrier at the ZnPc/Cu interface for case 3. In Fig. 10, the reverse current density is much greater for case 3 than for case 4, which suggests that the Schottky-barrier height at the GZO/ZnPc interface is less for case 3 than for case 4. The current density for case 3 (Fig. 10) is much greater than that for case 2 immediately after device preparation (Fig. 3), even though the rectification ratio is poor in both cases. This suggests that the Schottky-barrier heights at the GZO/ZnPc and the ZnPc/Cu interfaces are lower for case 3 than for case 2.

B. Mechanism for the change in Schottky-barrier height

As discussed in Sec. IV A, the effects of aging and illumination are explained mainly by the change in Schottky-barrier height at the ZnPc/Cu interface. In general, there are three mechanisms for this change. (1) The work function of the electrode is shifted due to oxide formation.²⁶ (2) Pinning levels are generated at the organic/electrode interface to which the Fermi level of the electrode is pinned.^{15,27,28} (3) An electric dipole layer is induced at the organic/electrode interface, which causes a shift of the vacuum level at the surface of the organic layer relative to that of the electrode.²⁹ In the aged cell, the Schottky-barrier height at the ZnPc/Cu interface was decreased by illumination, but the decreased barrier height slowly increased when the cell was placed in the dark. This result is not explained by mechanism (1) because a metal oxide is usually stable once it is formed. Mechanism (2) is not applicable to the present case because the generation of the pinning levels by illumination and the disappearance of pinning levels in the dark are unrealistic.

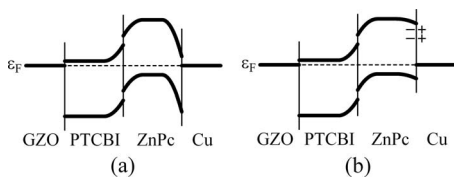


FIG. 11. Proposed energy band diagrams for cell A under white-light illumination with $V_{\text{bias}}=0$ V (a) immediately after device preparation and (b) after aging in air.

The most probable explanation of the present results is mechanism (3). During aging, electron trapping levels could be generated at the surface of the ZnPc layer facing to the Cu layer. On illumination, the photogenerated electrons are trapped in these levels and the countercharges collect on the surface of the Cu layer, resulting in an electric dipole layer at the ZnPc/Cu interface. The mutually trapped negative and positive charges are not stable, so they dissociate slowly after the light is turned off. The dipole layer produces a large electric field at the ZnPc/Cu interface. This explains the large EA signal for the surface of the ZnPc layer in case 4.

C. Mechanism of the aging effect for cell A

The improvement in η for cell A [Fig. 2(a)] can be explained in a similar manner. Since the photocurrent-voltage measurement for Fig. 2(a) was carried out under illumination of a white light of 100 mW/cm^2 , the band diagrams in Fig. 11 are applicable. Immediately after device preparation, a large electric field exists near the ZnPc/Cu interface that blocks the hole transport to the Cu electrode. After aging in air, the hole-blocking electric field is nearly quenched by white-light illumination, resulting in a significant improvement in η . In cell A, two photovoltaic cells are connected in series: one is the PTCBI/ZnPc heterojunction cell and the other is the ZnPc/Cu Schottky-barrier cell. However, the carrier generation by the electric field near the ZnPc/Cu interface does not play an important role because carrier generation near the PTCBI/ZnPc interface is much more effective. The improvement in rectification ratio on aging [Fig. 2(b)] is also explained by the band diagrams in Fig. 11. The measurement for Fig. 2(b) was carried out immediately after white-light illumination, so the band diagrams in Fig. 11 are also applicable. For the as-prepared device, the Schottky-barrier height at the ZnPc/Cu interface is large, so that hole injection from the Cu electrode is suppressed resulting in a small forward current. By contrast, the reverse current is relatively large because electron injection from Cu to the LUMO level of ZnPc is relatively easy under the reverse bias condition. However, after aging, the forward current increases because the barrier for hole injection from the Cu electrode decreases, whereas the reverse current decreases because a large electron-injection barrier is formed at the ZnPc/Cu interface.

V. CONCLUSIONS

The photovoltaic properties of cell A (GZO/PTCBI/ZnPc/Cu) showed a significant aging effect in open air. After aging for 24 days, η improved to 0.46 % from an initial

value of 0.02 %. To elucidate the mechanism of this aging effect, detailed studies were performed for cell B (GZO/ZnPc/Cu). The results reveal that a tall Schottky barrier existed at the ZnPc/Cu interface immediately after device preparation, which blocks the transport of photogenerated holes to the Cu electrode. This is why η of as-prepared cell A was very low. White-light illumination of the aged device decreased the Schottky-barrier height at the ZnPc/Cu interface, resulting in a drastic improvement in η . When the light was turning off, the barrier height returned to the greater value with a time constant of ~ 1 h in air and ~ 10 h in vacuum. The most probable mechanism for the change in Schottky-barrier height at the ZnPc/Cu interface is the formation of electron traps at the surface of the ZnPc layer facing the Cu electrode on aging, which trap electrons photogenerated by white-light illumination. Thus, it has been demonstrated that a Cu anode has a specific property whereby the junction with the donor layer becomes nearly Ohmic under or immediately after illumination by strong light of $\sim 100 \text{ mW/cm}^2$ in intensity.

- ¹H. Spanggaard and F. C. Krebs, *Sol. Energy Mater. Sol. Cells* **83**, 125 (2004).
- ²A. J. Mozer and N. S. Sariciftci, in *Thin Film Solar Cells, Fabrication, Characterization and Application*, edited by J. Poortmans and V. Arkhipov (Wiley, Chichester, 2006), Chap. 10.
- ³C. W. Tang, *Appl. Phys. Lett.* **48**, 183 (1986).
- ⁴N. S. Sariciftci, D. Braun, C. Zhang, V. I. Srdanov, A. J. Heeger, G. Stucky, and F. Wudl, *Appl. Phys. Lett.* **62**, 585 (1993).
- ⁵S. Morita, S. B. Lee, A. A. Zakhidov, and K. Yoshino, *Mol. Cryst. Liq. Cryst.* **256**, 839 (1994).
- ⁶P. Peumans and S. R. Forrest, *Appl. Phys. Lett.* **79**, 126 (2001); **80**, 338(E) (2002).
- ⁷M. Hiramoto, H. Fujiwara, and M. Yokoyama, *J. Appl. Phys.* **72**, 3781 (1992).
- ⁸K. Suemori, T. Miyata, M. Hiramoto, and M. Yokoyama, *Jpn. J. Appl. Phys., Part 2* **43**, L1014 (2004).
- ⁹G. Yu, K. Pakbaz, and A. J. Heeger, *Appl. Phys. Lett.* **64**, 3422 (1994).
- ¹⁰J. Y. Kim, S. H. Kim, H. Lee, K. Lee, W. Ma, X. Gong, and A. J. Heeger, *Adv. Mater. (Weinheim, Ger.)* **18**, 572 (2006).
- ¹¹Y. Yoshida, S. Tanaka, I. Hiromitsu, Y. Fujita, and K. Yoshino, *Jpn. J. Appl. Phys.* **47**, 867 (2008).
- ¹²J. A. Chaney and P. E. Pehrsson, *Appl. Surf. Sci.* **180**, 214 (2001).
- ¹³J. Owen, M. S. Son, K.-H. Yoo, B. D. Ahn, and S. Y. Lee, *Appl. Phys. Lett.* **90**, 033512 (2007).
- ¹⁴T. Maki and H. Hashimoto, *Bull. Chem. Soc. Jpn.* **25**, 411 (1952).
- ¹⁵C. M. Heller, I. H. Campbell, D. L. Smith, N. N. Barashkov, and J. P. Ferraris, *J. Appl. Phys.* **81**, 3227 (1997).
- ¹⁶P. A. Lane, J. Rostalski, C. Giebeler, S. J. Martin, D. D. C. Bradley, and D. Meissner, *Sol. Energy Mater. Sol. Cells* **63**, 3 (2000).
- ¹⁷L. Sebastian, G. Weiser, and H. Bässler, *Chem. Phys.* **61**, 125 (1981).
- ¹⁸I. Hiromitsu and G. Kinugawa, *Jpn. J. Appl. Phys., Part 1* **44**, 60 (2005).
- ¹⁹M. Nonomura, I. Hiromitsu, and S. Tanaka, *Appl. Phys. Lett.* **88**, 042111 (2006).
- ²⁰S. Tanaka, Y. Yoshida, M. Nonomura, K. Yoshino, and I. Hiromitsu, *Thin Solid Films* **516**, 1006 (2008).
- ²¹I. Hiromitsu, Y. Murakami, and T. Ito, *J. Appl. Phys.* **94**, 2434 (2003).
- ²²I. Hiromitsu and G. Kinugawa, *Synth. Met.* **153**, 73 (2005).
- ²³I. Hiromitsu, S. Mada, A. Inoue, Y. Yoshida, and S. Tanaka, *Jpn. J. Appl. Phys., Part 1* **46**, 7241 (2007).
- ²⁴H. B. Michaelson, *J. Appl. Phys.* **48**, 4729 (1977).
- ²⁵S. Sze, *Physics of Semiconductor Devices*, 2nd ed. (Wiley, New York, 1981), Chap. 5.
- ²⁶J. Ghijsen, L. H. Tjeng, J. van Elp, E. Eskes, J. Westerink, G. A. Sawatzky, and M. T. Czyzyk, *Phys. Rev. B* **38**, 11322 (1988).
- ²⁷C. Shen and A. Kahn, *Org. Electron.* **2**, 89 (2001).
- ²⁸S. Braun and W. R. Salaneck, *Chem. Phys. Lett.* **438**, 259 (2007).
- ²⁹H. Ishii, K. Sugiyama, E. Ito, and K. Seki, *Adv. Mater. (Weinheim, Ger.)* **11**, 605 (1999).